RSC Medicinal Chemistry

ROYAL SOCIETY OF CHEMISTRY

RESEARCH ARTICLE

View Article Online
View Journal

Cite this: DOI: 10.1039/d6md00300a

Triarylphosphonium-conjugated Sn(IV)-porphyrins for antimicrobial photodynamic therapy: impact of substituents on lipophilicity, aggregation, and photoantibacterial activity

Gayathri MP, [a] Nandhakumar Muruganandam, [b] Sutharsan Govindarajan *[b] and Balaji Babu *[a]

Received 16th April 2026,
Accepted 19th May 2026

DOI: 10.1039/d6md00300a

rsc.li/medchem

Antimicrobial photodynamic therapy is an effective approach to counteract bacterial infections that are not possible to be treated through antibiotics. In this study, three cationic Sn(IV) porphyrins bearing triaryl phosphonium substituents (**SnP1**, **SnP2**, and **SnP3**) were synthesized and evaluated as antibacterial photosensitizers (PSs). All compounds exhibited efficient singlet oxygen generation with quantum yields (Φ_Δ) in the range of 0.72–0.78. Aggregation studies show reduced aggregation of **SnP1** and **SnP2** than **SnP3**. Lipophilicity (log *P*) values indicated that **SnP2**, containing fluoro substituents, possesses a balanced amphiphilic character favorable for effective bacterial uptake and antimicrobial activity. The photodynamic antibacterial activity (427 nm LED; 22 mW cm^{-2}) of **SnP1**, **SnP2** and **SnP3** was evaluated against *Escherichia coli* (*E. coli*) and clinical methicillin-resistant *Staphylococcus aureus* (MRSA). **SnP2** exhibited significant photoantimicrobial activity against both Gram-negative (*E. coli*) and Gram-positive (MRSA) bacteria with a log reduction of 8.7 at 10 μM and 8.5 at 20 nM, respectively. Overall, our study highlights the importance of structural tuning of lipophilicity and aggregation in enhancing the efficacy of Sn(IV)-porphyrin-based photosensitizers.

1. Introduction

The growing threat of antimicrobial resistance has prompted global health agencies to identify priority pathogens that require urgent therapeutic intervention. The World Health Organization recently released the Indian Priority Pathogen List (IPPL), which highlights several clinically significant bacteria.[1] Among these, *Escherichia coli* (*E. coli*), *Klebsiella pneumoniae*, *Acinetobacter baumannii* and *Pseudomonas aeruginosa* are recognized as critical priority pathogens. In addition, high-priority pathogens include *Staphylococcus aureus* (particularly MRSA), *Enterococcus* species, and *Salmonella* species (typhoidal and non-typhoidal).[1,2]

Although a wide range of antimicrobial strategies have been developed, there is still a critical need for treatment that can reduce or suppress antibiotic resistance. In this context, oxidative stress-based antimicrobial methods have attracted considerable attention.[3] These approaches generate reactive oxygen species (ROS) that damage key cellular components, leading to microbial cell death.[3,4] The multi-target oxidative action of aPDT minimizes resistance development, making it effective against multidrug-resistant pathogens.[5]

In aPDT, upon light absorption, the photosensitizer (PS) undergoes electronic excitation from the ground state to a higher-lying excited state, subsequently transferring energy to molecular oxygen to generate ROS. Its efficacy is governed by molecular design, which dictates absorption properties, excited-state dynamics, ROS yield, and interactions with microbial cells.[6] These ROS induce oxidative damage to key cellular components, resulting in irreversible cellular damage and microbial cell death. Among various classes of photosensitizers investigated to date, tin(IV)-based porphyrins represent one of the most versatile and widely studied scaffolds for photodynamic applications.[7] Sn(IV)-porphyrins with trans axial ligands inhibit the π–π interactions of porphyrin macrocycles and minimize aggregation. In addition, Sn(IV)-porphyrins exhibit strong absorption in the visible region (420–440 nm), facilitate intersystem crossing (ISC) thereby enhancing triplet-state yields, and efficiently generate singlet oxygen, making them highly suitable candidates for aPDT.[7,8] Moreover, the porphyrin macrocycle provides a chemically flexible scaffold that allows systematic modification of peripheral substituents to fine tune the physicochemical properties

[a] *Department of Chemistry, SRM University-AP, India.*
E-mail: balaji.b@srmap.edu.in
[b] *Department of Biological Sciences, SRM University-AP, India.*
E-mail: sutharsan.g@srmap.edu.in

such as lipophilicity, aggregation behaviour, and interaction with microbial cells.

For antimicrobial applications, efficient interaction between the photosensitizer and microbial cell surfaces is a critical determinant of photodynamic activity. Bacterial cell envelopes typically possess a net negative charge, which favours the interaction of cationic photosensitizers through electrostatic attraction. As a result, cationic porphyrin derivatives have shown enhanced antimicrobial photodynamic activity due to improved binding and uptake by microbial cells.[9] However, increasing hydrophobicity to enhance membrane interactions can also promote aggregation in aqueous environments, which often reduces antimicrobial photodynamic efficiency due to self-quenching of excited states. Therefore, achieving a balanced combination of charge, lipophilicity, and molecular dispersion is essential for optimizing antimicrobial photodynamic performance. The choice of the wavelength of light to activate a photosensitizer largely depends on the depth of infection. Blue light is well suited for superficial or topical infections, while red light is preferred for deep infections as it has better tissue penetration.[4,5] Porphyrins with intense absorption (Soret band) in the blue region of the spectrum are well-suited candidates as photosensitizers for topical bacterial infections.

In this context, attaching triaryl phosphonium ($TArP^+$) moieties can be a promising strategy for modulating the lipophilic nature and aggregation behaviour of photosensitizers.[10] The positive charge on the triaryl phosphonium group can enhance interactions with microbial membranes through electrostatic interactions of negatively charged microbial membranes while simultaneously influencing the hydrophobic character of the photosensitizer. In the present study, we investigate a series of triaryl phosphonium-conjugated Sn(IV)-porphyrin photosensitizers (**SnP1–SnP3**) (Fig. 1a) designed to modulate lipophilicity, aggregation behaviour, and antimicrobial photodynamic activity towards Gram-negative *Escherichia coli* and Gram-positive methicillin-resistant *Staphylococcus aureus* (MRSA). By correlating molecular structure with photophysical and biological properties, this work provides insights into the structure–activity relationships governing phosphonium-based porphyrin photosensitizers and highlights their potential as promising agents for antimicrobial photodynamic therapy.

2. Results and discussion

2.1. Synthesis and characterisation

The Sn(IV)-complexes (**SnP1–SnP3**) were prepared by stirring the corresponding free-base porphyrins[11] with $SnCl_2{\cdot}H_2O$ at 60 °C for 6 h and purified by neutral alumina chromatography (Scheme S1). The structures of the Sn(IV)-complexes were confirmed by NMR (^1H, ^{31}P, and ^{19}F NMR) and mass spectrometry (Fig. S1–S6). The β-hydrogens of the porphyrin core were observed around

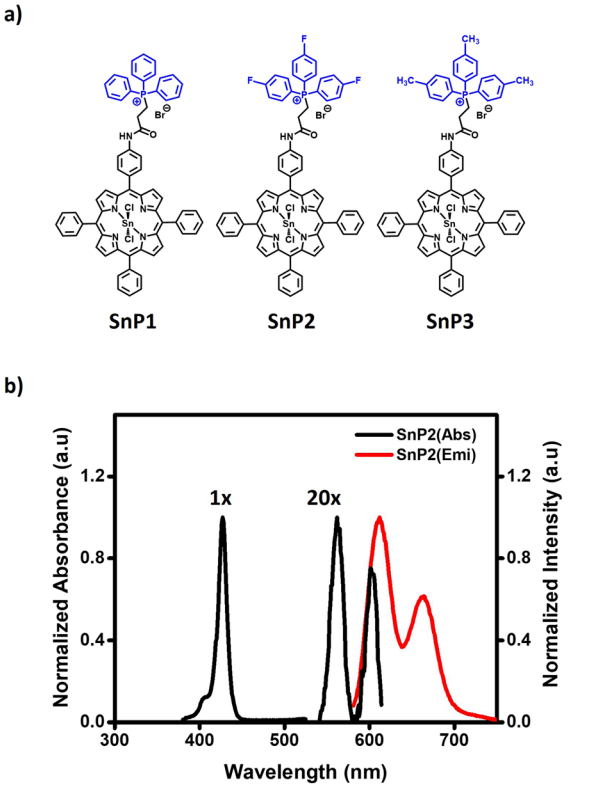

Fig. 1 (a) Schematic representation of Sn(IV)-porphyrins studied; (b) absorption (black) and emission (red) spectra of **SnP2** in DMF.

9.11 ppm, while the aryl protons of the triarylphosphonium moiety appeared in the aromatic region (7.7–8 ppm). Signals corresponding to the aliphatic linker were detected around 3.2–3.5 ppm. The amide (NH) proton resonated downfield at 10.9 ppm consistent with reported literature values.[11] Furthermore, the ^{31}P-NMR spectra of the Sn(IV)-complexes showed characteristic peaks around 25 ppm, which are downshifted from the free triaryl phosphines confirming successful conjugation (Fig. S1–S3). The ^{19}F-NMR spectrum of **SnP2** displayed fluorine peaks at −98.15 ppm. The mass spectral analysis revealed peaks corresponding to the [M-2Cl + H] fragment.

2.2. Photophysical properties

The electronic absorption spectra of Sn(IV)-porphyrins (**SnP1**, **SnP2** and **SnP3**) (Fig. 1b and S7) show a typical intense Soret band at 428 nm ($S_0 \rightarrow S_2$ transition) and two Q-bands around 563 and 605 nm ($S_0 \rightarrow S_1$ transition) typical of Sn(IV)-porphyrin systems.[7,11,12] All three Sn(IV)-porphyrins exhibited a similar pattern in UV-vis, indicating that triarylphoshonium substitution has minimal impact on the electronic properties because of the aliphatic linkers. The emission spectra of Sn(IV)-porphyrins (**SnP1–SnP3**) displayed two emission bands around 610 and 662 nm when excited at 428 nm (Fig. 1b and S7). The fluorescence quantum yields (Φ_F) of Sn(IV)-porphyrins were low (0.029). The

Table 1 Selected photo physicochemical properties of **SnP1**–**SnP3** in DMF

	SnP1	SnP2	SnP3
$\lambda_{max/nm}$ (log ε)	428(5.11), 562(3.75), and 605(3.66)	428(5.06), 563(3.70), and 603(3.57)	428(5.10), 564(3.71), and 605(3.61)
λ_{em} [a]	613, 662	612, 661	612, 662
Φ_F [b]	0.029	0.026	0.029
Φ_Δ [c]	0.72	0.78	0.76
log $P_{(o/w)}$	0.31	0.28	0.35

[a] Excitation at the B (or Soret) band maxima. [b] ZnTPP = 0.033 in DMF.[16] [c] ZnTPP in DMF.[30]

relatively low quantum yield values are consistent with typical Sn(IV)-porphyrin systems, where efficient intersystem crossing from the singlet-excited state to the triplet state occurs.[13] The photophysical property results of all three compounds are summarized in Table 1. The singlet oxygen generating ability of the synthesised Sn(IV)-porphyrins was evaluated using 9,10-dimethylanthracene (DMA) as a singlet oxygen trap.[14] DMA is also widely employed as a singlet oxygen probe. It reacts with singlet oxygen to form a stable endoperoxide, leading to a decrease in its characteristic absorption. Monitoring this decrease spectroscopically allows indirect detection and quantification of singlet oxygen generation by a comparative method.[32] The singlet oxygen quantum yield (Φ_Δ) measurements indicate that all three Sn(IV)-porphyrins are efficient singlet oxygen generators upon irradiation. The control experiments in the dark displayed negligible $^1O_2$ generation. The singlet oxygen ($^1O_2$) lifetime is higher in organic solvents than in water and physiological environments. The fate of singlet oxygen is further governed by biomolecular quenching, oxygen availability, and cellular microenvironmental effects. Therefore, the Φ_Δ value measured by the DMA method primarily represents intrinsic photosensitising efficiency under idealized conditions and may not directly correlate with $^1O_2$ generation efficiency under physiological conditions.

2.3. Aggregation studies

Porphyrins and metalloporphyrins tend to aggregate in an aqueous or physiological medium due to either H or J-aggregation.[15] Sn(IV) porphyrins with suitable bulky trans-axial ligands are known to suppress H-aggregation

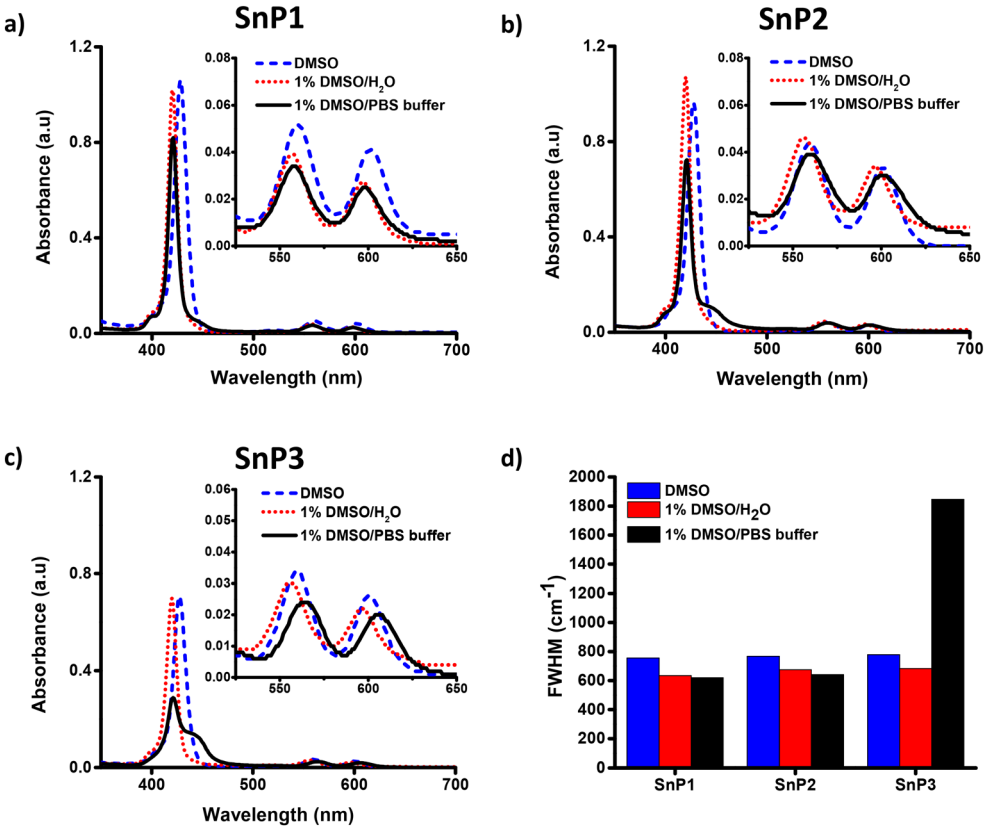

Fig. 2 Aggregation studies: UV-visible spectra of a) **SnP1**, b) **SnP2**, and c) **SnP3** in DMSO, 1% DMSO/H_2O, and 1% DMSO/PBS buffer (inset: expanded Q-bands); d) FWHM (cm^{-1}) in DMSO (blue), 1% DMSO/H_2O (red) and 1% DMSO/PBS buffer (black).

by sterically hindering the close approach of adjacent porphyrin units, whereas those with simple axial ligands such as Cl or OH tend to exhibit some degree of aggregation in aqueous solution.[7,8] Aggregation significantly reduces the photodynamic efficiency of photosensitizers by quenching their excited states and decreasing singlet oxygen generation.[15,17,18] Therefore, maintaining the photosensitizer in a monomeric form is essential for efficient ROS production and effective antimicrobial photodynamic therapy (aPDT). The aggregation behaviour of the three Sn(IV)-porphyrin derivatives (**SnP1**–**SnP3**) was evaluated by measuring their UV-visible absorption spectra in DMSO, 1% DMSO/PBS, and 1% DMSO/water (Fig. 2a–c). In DMSO, all three compounds displayed a narrow and intense Soret band around 428 nm along with well-resolved Q-bands in the 520–610 nm region, suggesting that the Sn(IV)-porphyrins are present in a monomeric and well-dispersed form in this solvent. In 1% DMSO/H_2O, a slight blue shift (420 nm) in the Soret band is observed for all three Sn(IV)-porphyrins; however, the band remained sharp with a similar full-width-half-maximum (FWHM) value (Fig. 2d). Full-width-half-maximum (FWHM) is the width of a spectral peak measured at half of its maximum intensity, indicating peak sharpness and providing insight into aggregation and the molecular environment.[7,8] This suggests that the Sn(IV)-porphyrins remain predominantly in the monomeric form in 1% DMSO/H_2O. This behaviour is attributed to the cationic triarylphosphonium moiety, which increases solubility. Interestingly in 1% DMSO/PBS, for **SnP1** and **SnP2**, a decrease in Soret band absorption is observed but the band remained narrow with a similar FWHM. In the case of **SnP3**, a significant decrease in Soret band absorption is observed along with peak broadening. A new red-shifted absorption band appeared with an increased FWHM. This behaviour suggests that some degree of J-aggregation is induced for **SnP3** in 1% DMSO/PBS.[18] This is attributed to the increased hydrophobic nature contributed by the tritolylphosphonium moiety in **SnP3**; additionally, the ionic strength in PBS aids in decreasing solubility and increasing aggregation.[19] This study shows how a small change in substituents on the triphenylphosphonium (TPP^+) moiety can strongly influence the aggregation behaviour of Sn(IV)-porphyrins because they alter the steric and hydrophobic properties of the molecule.

2.4. Lipophilicity

The uptake and interaction of porphyrins with bacterial membranes depends on lipophilicity. This property directly influences antimicrobial photodynamic activity, as we have observed in our previous studies.[20] Balanced lipophilicity helps in minimizing aggregation and maintaining solubility. The lipophilicity of the synthesized Sn(IV)-porphyrin derivatives was evaluated by determining their octanol/water partition coefficients ($\log P$) (Table 1).[21,29] The obtained values were 0.31 for **SnP1**, 0.28 for **SnP2**, and 0.35 for **SnP3**, indicating that all three compounds possess moderate lipophilicity with partial water solubility. Among the three derivatives, **SnP3** exhibits the highest $\log P$ value, which is likely due to the methyl substituents present in **SnP3** that increase its hydrophobicity. In contrast, **SnP2** shows the lowest $\log P$ value, likely due to the fluorine substituents, which slightly increase the polarity of the molecule and reduce its affinity for the organic phase. **SnP1** displays an intermediate $\log P$ value.

2.5. Photoantimicrobial activity against Gram (−) *E. coli* and the Gram (+) clinical pathogen – MRSA

Blue-light-absorbing photosensitizers are advantageous for treating bacterial skin infections because blue light (400–450 nm) penetrates sufficiently into superficial tissues, where most skin infections occur.[22] Sn(IV)-porphyrins are ideal photosensitizers since they strongly absorb in the blue region (Soret band) and produce singlet oxygen efficiently. The antimicrobial photodynamic activities of the triaryl phosphonium-based photosensitizers **SnP1**–**SnP3** were evaluated against *E. coli* (Gram −) and a clinical isolate of methicillin-resistant *S. aureus* (MRSA) (Gram +) (Fig. 3 and 4 and S8). The Sn(IV)-porphyrins exhibited concentration-dependent antibacterial activity under light exposure (427 nm LED). Significant differences in photoantibacterial efficacy were observed among the three compounds depending on the bacterial species. The log reduction numbers are calculated using the expression: log reduction = $\log_{10}(A_0) - \log_{10}(A_{30})$, where A_0 and A_{30} correspond to the number of viable microorganisms at 0 and 30 min of light exposure, respectively (Table 2). In accordance with the established antimicrobial efficacy criteria, a log reduction exceeding 3 log units (≥99.9%) was deemed as the threshold for significant antibacterial activity.[31] In *E. coli*, **SnP1** and **SnP2** exhibited the highest photoantibacterial activity at 10 μM, with log reductions of 8.7 for both the compounds. At a concentration of 7.5 μM, the log reductions are 4.13 and 5.65, respectively, for **SnP1** and **SnP2**. In contrast, **SnP3** showed lower photoantibacterial activity at the tested concentration, producing a log reduction of 3.7 at 10 μM. Interestingly, in MRSA, these compounds exhibited strong photoantibacterial activity at nanomolar concentrations. **SnP1** and **SnP3** showed similar photoantibacterial activity at 20 nM (Fig. 3 and S8), producing a log reduction of 5.4, whereas **SnP2** exhibited the highest photoantibacterial activity with a log reduction of 8.49 and completely inhibited bacterial growth at 20 nM. Overall, among the three compounds, **SnP2** presents the highest aPDT activity followed by **SnP1** and **SnP3** (Fig. 4c, e and S8). The difference in the aPDT activity between Gram (−)- and Gram (+)- bacteria can be attributed to the presence of an additional outer membrane in Gram-negative *E. coli*, which acts as a permeability barrier and may limit the uptake of the photosensitizers.[23] Consistent with

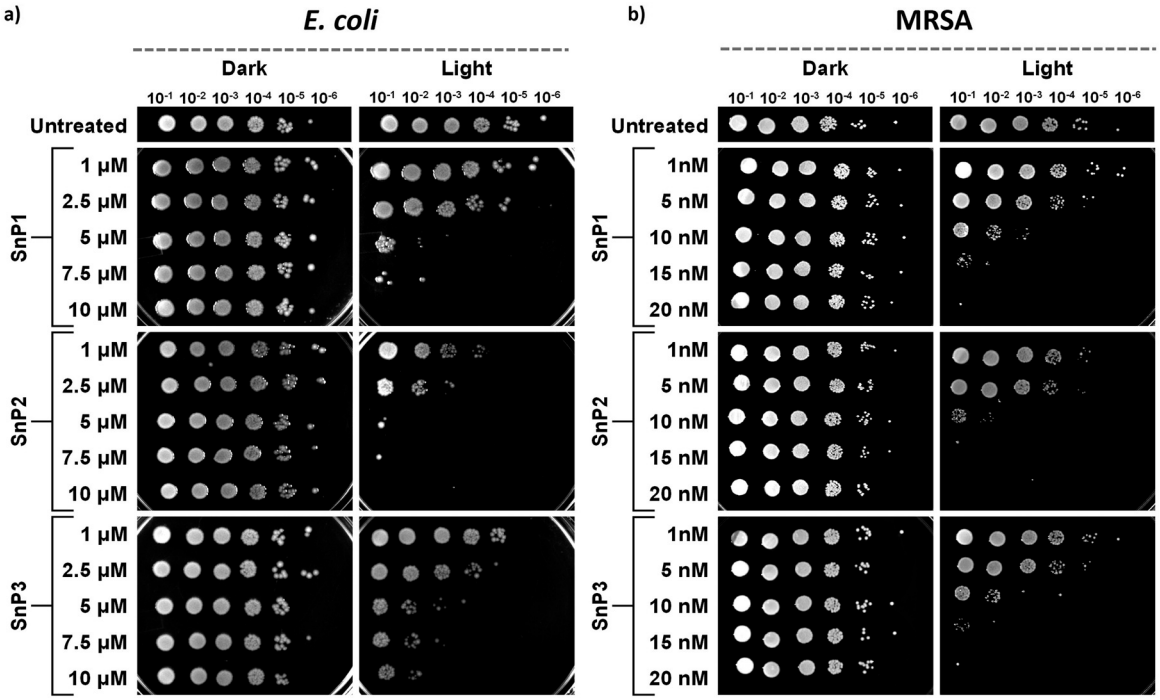

Fig. 3 Antibacterial activity of **SnP1**, **SnP2**, and **SnP3** both under dark and light exposure (427 nm LED; 30 min; 40 J cm^{-2}) conditions at different concentrations against (a) *E. coli* and (b) MRSA by spot dilution assay.

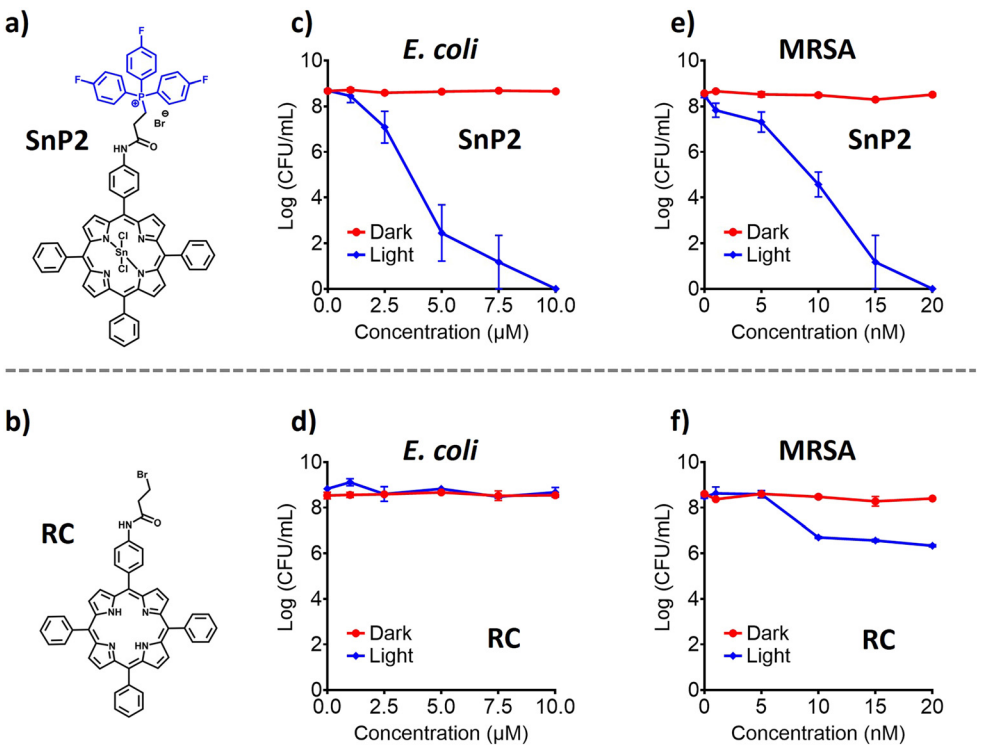

Fig. 4 Chemical structures and antibacterial activity of the compounds. (a) **SnP2** and (b) reference compound (**RC**). Antibacterial activity against *E. coli* (c and d) and MRSA (e and f) under dark (red) and light irradiation (blue) conditions with a 427 nm LED (22 mW cm^{-2}; 30 min; 40 J cm^{-2}) at different concentrations.

their photoactivatable nature, all the three Sn(IV)-porphyrins showed negligible toxicity at all concentrations tested against *E. coli* and MRSA under dark conditions. However, a notable feature of **SnP2** is that its light-activated antibacterial effects

Table 2 Log reduction of *E. coli* and MRSA treated with **SnP1**–**SnP3** with 10 μM and 20 nM, respectively. In the dark and 427 nm light irradiation (22 mW cm^{-2}; 40 J cm^{-2}) for 30 min

	Log reduction (% of survival)			Log reduction (% of survival)		
	Dark			Light		
Bacteria	**SnP1**	**SnP2**	**SnP3**	**SnP1**	**SnP2**	**SnP3**
E. coli[a]	<0.1 (97.6)	<0.1 (95.3)	<0.1 (90.7)	8.6 (0)	8.7 (0)	3.7 (0)
MRSA[b]	<0.1 (91.1)	<0.1 (88.2)	<0.1 (91.1)	5.4 (0)	8.5 (0)	5.4 (0)

[a] 10 μM Sn(IV)-porphyrins. [b] 20 nM Sn(IV)-porphyrins.

are more pronounced compared to those of Sn(IV)-porphyrins reported previously in the literature.[7,24] The low dark toxicity and high light-induced toxicity are one of the main criteria for effective photosensitizers (PSs) for aPDT. A control experiment with porphyrin, a reference compound (**RC**) (Fig. 4b) without the triphenylphosphonium moiety, showed negligible toxicity under both dark and light conditions within the same concentration range studied against *E. coli* and MRSA (Fig. 4d and f). The combined results of aggregation studies, singlet oxygen generation and light-induced toxicity collectively demonstrate that Sn(IV)-porphyrins (**SnP1**–**SnP3**) possess promising potential as photosensitizers for antimicrobial photodynamic therapy (aPDT).

2.6. Fluorescence microscopy localization studies

Sn(IV)-porphyrins (**SnP1**–**SnP3**) are relatively emissive, and this property can be exploited to investigate their localisation and accumulation in bacterial cells under both dark and photodynamic conditions (Fig. 5 and S9). Based on the toxicity profile in the dark, fluorescence imaging studies were performed at 10 μM and 20 nM concentrations of Sn(IV)-porphyrins for *E. coli* and MRSA, respectively. Fluorescence microscopy images of *E. coli* and MRSA were captured upon incubation with Sn(IV)-porphyrins along with DAPI, a DNA-binding dye (Fig. 5 and S9). Under dark conditions, the photosensitizers were predominantly accumulated at the membrane, in addition to cytoplasmic localisation, of *E. coli*. However, in MRSA, a weak or no fluorescence signal was observed. In both cases, DAPI staining revealed a smooth bacterial nucleoid morphology, similar to that in the untreated control, indicating that Sn(IV)-porphyrins do not induce any DNA damage under dark conditions.

Upon light activation, Sn(IV)-porphyrins exhibited enhanced red fluorescence signals both in *E. coli* and MRSA (Fig. 5). In both cases, no visible damage to the cell membrane was observed. However, DAPI staining showed a distorted and condensed nucleoid, indicative of photodynamic activation and DNA damage. The cells treated with **SnP1** and **SnP3** showed phenotypic changes similar to those observed with **SnP2** (Fig. S9). These red fluorescence signals indicate cellular uptake of the compounds. In *E. coli*, fluorescence was observed only in a subset of cells, whereas in MRSA nearly all cells exhibited strong fluorescence, suggesting more efficient uptake of the compounds by MRSA compared to *E. coli*. This observation correlates with the higher light-induced antimicrobial activity observed in MRSA relative to *E. coli*.

2.7. Intracellular ROS production

Next, we studied the intracellular ROS generating ability of synthesized photosensitizers by the DCFDA (2′,7;-dichlorofluorescein diacetate) assay.[25] DCFDA is

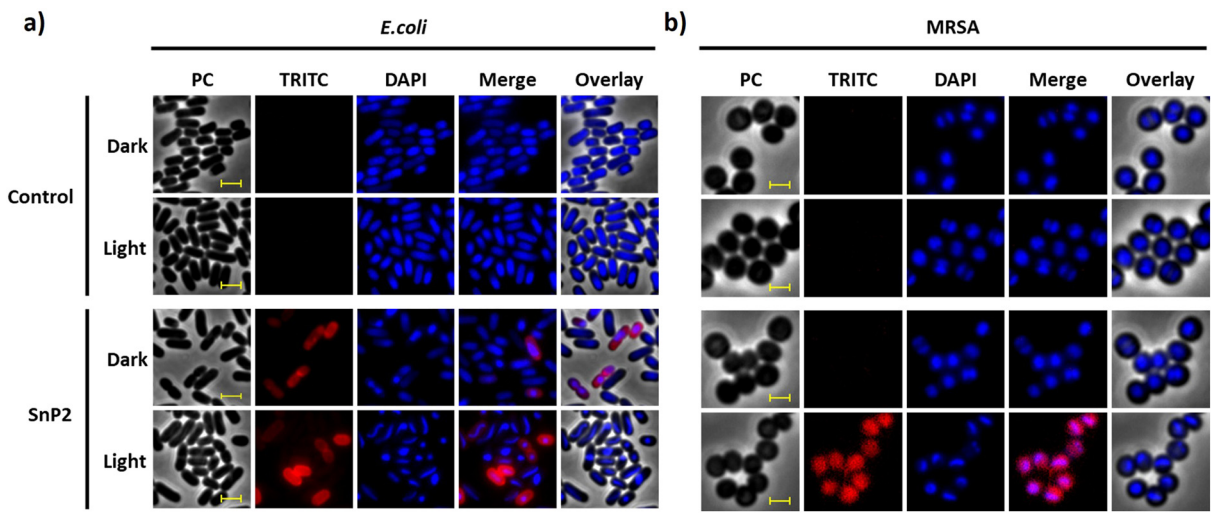

Fig. 5 Fluorescence microscopy images of (a) *E. coli* treated with 10 μM of **SnP2** in the dark and after light exposure (427 nm LED, 22 mW cm^{-2}); (b) MRSA treated with 20 nM of **SnP2** under dark and after light exposure (427 nm LED, 22 mW cm^{-2}) conditions. Localization of the **SnP2** compound was observed in the TRITC filter of fluorescence microscopy, and the cells were observed using phase contrast (PC) microscopy. PC images (grey), DAPI fluorescence (blue) and compound fluorescence (red) are shown in individual panels. The scale bar corresponds to 2 μm.

non-emissive cell-permeable dye that undergoes deacetylation to form DCFH, a non-fluorescent intermediate. DCFH non-specifically reacts with any reactive oxygen species and is oxidised to DCF (2′,7;-dichlorofluorescein), a highly green emissive compound.[26] *E. coli* and MRSA were incubated with **SnP2** and DCFDA, and kept under dark and light conditions. The fluorescence microscopy images of the bacteria (*E. coli* and MRSA) display no visible green emission from the cells kept under dark conditions (Fig. 6). Interestingly, a pronounced increase in green fluorescence was observed in bacteria preincubated with **SnP2** upon light exposure indicating efficient intracellular ROS generation. Control experiments in *E. coli* and MRSA under dark and light conditions in the absence of **SnP2** exhibited no detectable green fluorescence (Fig. 6). These results confirm that **SnP2** induces light-triggered ROS generation within the bacterial cells.

3. Conclusion

In conclusion, three triaryl phosphonium-substituted Sn(IV) porphyrins (**SnP1**, **SnP2**, and **SnP3**) were successfully synthesized and characterized. The influence of substituents on the triphenyl phosphonium groups was systematically investigated in terms of aggregation behaviour, lipophilicity, and antimicrobial photodynamic activity. Among the three compounds, **SnP2** exhibited the most balanced lipophilicity with reduced aggregation and enhanced antimicrobial activity against both *E. coli* and MRSA, highlighting the importance of structural modification in optimizing photodynamic efficiency. Thus, fine-tuning substituent effects on phosphonium porphyrins is an effective strategy for developing potent Sn(IV)-porphyrin-based photosensitizers for antimicrobial photodynamic therapy. Further structural refinement of Sn(IV) porphyrins *via meso*-substitution can be strategically employed to enhance aqueous solubility, thereby enabling more comprehensive *in vitro* and *in vivo* evaluation. Moreover, the *trans*-dichloro axial coordination sites serve as a synthetically accessible platform for ligand exchange, facilitating the incorporation of suitable axial ligands that can improve water solubility and enable the introduction of targeting moieties, ultimately enhancing cellular uptake and antimicrobial photodynamic efficacy.

4. Experimental

4.1. Materials

Benzaldehyde and triphenylphosphine were obtained from Hyma (India), tris(4-fluorophenyl)phosphine, tri(*p*-tolyl)-phosphine and 2′,7′-dichlorofluorescein diacetate (DCFDA) were obtained from BLD Pharma. 3-Bromo-*N*-(4-(10,15,20-triphenylporphyrin-5-yl)phenyl)propenamide was synthesized according to literature procedures.[27,28] *E. coli* (MG1655) and methicillin-resistant *S. aureus* (MRSA) (ATCC43300) were used in this study. Bacterial strains were cultured in lysogeny broth (LB) and agar (1% tryptone (w/v), 0.5% yeast extract (w/v), 1% NaCl (w/v), and 2% agar/pH 7.2) were employed. For antibacterial assays, LB agar plates were prepared with

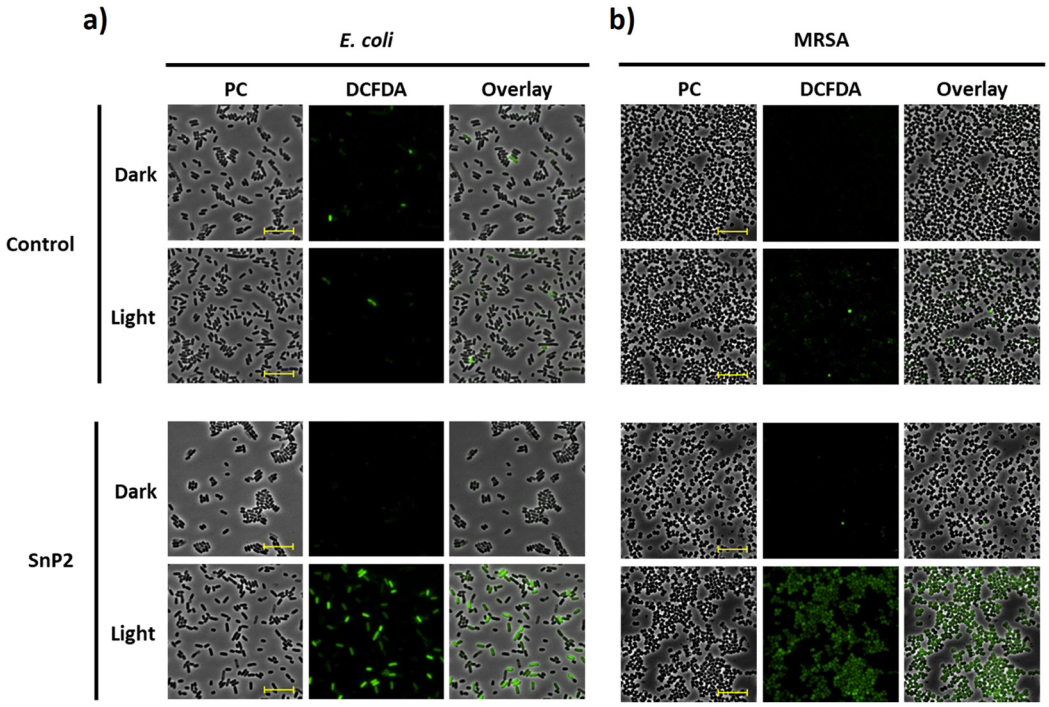

Fig. 6 DCFDA assay for intracellular ROS generation. Fluorescence microscopy images of (a) *E. coli* treated with 10 μM of **SnP2** under dark and light conditions along with controls; (b) MRSA treated with 20 nM of **SnP2** under dark and light conditions along with controls. Phase contrast (PC) (grey) and FITC filter (DCFDA) (green). The scale bar corresponds to 10 μm.

2% agar. For all experiments, bacteria were maintained at a temperature of 37 °C.

4.2. Methods

Detailed instrumentation and experimental protocols for bacterial work, fluorescence imaging and DCFDA studies are included in the SI.

4.3. Synthesis

The free-base porphyrins (**P1**–**P3**) were synthesized by following the previously reported procedure (Scheme S1).[28] The respective free-base porphyrins and $SnCl_2 \cdot H_2O$ were dissolved in dimethylformamide (DMF) and heated at 60 °C for 6 h. The completion of the reaction was monitored by TLC and UV-vis spectra. Then, the reaction mixture was added to ice-cold water to precipitate the compound. The precipitate was centrifuged and the supernatant was discarded. The crude pellet was washed with water to remove DMF and dried and purified by neutral alumina column chromatography (1% MeOH/$CHCl_3$) to give Sn(IV)-porphyrins (**SnP1**–**SnP3**) as purple solids in moderate yield.

SnP1. ^{1}H NMR ($CDCl_3$, 400 MHz): δ H 10.94 (s, 1H), 9.11 (m, 8H), 8.33 (dd, 6H), 8.19 (d, 2H), 8.01 (d, 2H), 7.76 (m, 24H), 3.75 (m, 2H), 3.24 (m, 2H); ^{31}P NMR ($CDCl_3$, 400 MHz): 23.87. MS (HRMS): *m*/*z* for $[M\text{-}2Cl + H]^+$ = 1064.41 (calc. 1064.81). UV-vis (λ/nm) in DMF: 428, 562, 605.

SnP2. ^{1}H NMR ($CDCl_3$, 400 MHz): δ H 10.64 (s, 1H), 9.11 (m, 8H), 8.32 (dd, 6H), 8.17 (d, 2H), 7.93 (d, 2H), 7.80 (m, 15H), 7.41 (m, 6H), 3.85 (m, 2H), 3.20 (m, 2H); ^{31}P NMR ($CDCl_3$, 400 MHz): 24.61; ^{19}F NMR ($CDCl_3$, 400 MHz): −98.15. MS (HRMS): *m*/*z* for $[M\text{-}2Cl + H]^+$ = 1118.41 (calc. 1118.78). UV-vis (λ/nm) in DMF: 428, 563, 603.

SnP3. ^{1}H NMR ($CDCl_3$, 400 MHz): δ H 10.95 (s, 1H), 9.12 (m, 8H), 8.34 (m, 6H), 8.19 (d, 2H), 8.09 (d, 2H), 7.84 (m, 9H), 7.64 (m, 6H), 7.54 (m, 6H), 3.63 (m, 2H), 3.20 (m, 2H), 2.50 (s, 9H); ^{31}P NMR ($CDCl_3$, 400 MHz): 25.01. MS (HRMS): *m*/*z* for $[M\text{-}2Cl + H]^+$ = 1106.42 (calc. 1106.89). UV-vis (λ/nm) in DMF: 428, 564, 605.

Author contributions

M. P. G. contributed to the synthesis of the molecules, photophysical properties, biological assays, and writing – original draft, review and editing. N. M. contributed to biological assays and writing – review and editing. B. B. & S. G. contributed to conceptualization, methodology, investigation, supervision, writing – review and editing, funding acquisition, and resources.

Conflicts of interest

There are no conflicts to declare.

Data availability

The data supporting this article have been included as part of the supplementary information (SI).

Supplementary information: detailed instrumentation and experimental protocols for bacterial work, fluorescence imaging and DCFDA studies are available in the SI. See DOI: https://doi.org/10.1039/d6md00300a.

Acknowledgements

M. P. G. and N. M. thank SRM University-AP for the Junior Research Fellowship and CSIR Direct-SRF (09/1354(23658)/2025-EMR-I), respectively. The authors acknowledge SRM University-AP, Andhra Pradesh, for their instrumentation facilities. B. B. acknowledges seed funding from SRM University-AP (SRMAP/URG/SEED/2023-24/011) and DST-FIST [SR-FST-CS-I-2021-219(C)] for supporting the Department of Chemistry at SRM University-AP. S. G. acknowledges funding from DST-SERB (CRG/2020/003295) and SRM University-AP (SRMAP/URG/GENERAL-D/2025-26/007).

References

1 H. Sati, E. Carrara, A. Savoldi, P. Hansen, J. Garlasco, E. Campagnaro, S. Boccia, J. A. Castillo-Polo, E. Magrini, P. Garcia-Vello, E. Wool, V. Gigante, E. Duffy, A. Cassini, B. Huttner, P. R. Pardo, M. Naghavi, F. Mirzayev, M. Zignol, A. Cameron, E. Tacconelli, A. Aboderin, M. Al Ghoribi, J. Al-Salman, A. Amir, A. Apisarnthanarak, M. Blaser, A. El-Sharif, S. Essack, S. Harbarth, X. Huang, G. Kapoor, G. Knight, J. C. Muhwa, D. L. Monnet, T. Ousassa, R. Sacsaquispe, J. Severin, M. Sugai, N. Taneja and A. Umubyeyi Nyaruhirira, *Lancet Infect. Dis.*, 2025, **25**, 1033–1043.
2 M. E. A. de Kraker, A. J. Stewardson and S. Harbarth, *PLoS Med.*, 2016, **13**(11), e1002184.
3 Á. Mourenza, J. A. Gil, L. M. Mateos and M. Letek, *Antioxidants*, 2020, **9**(5), 361.
4 M. J. Davies, *Biochem. Biophys. Res. Commun.*, 2003, **305**, 761–770.
5 G. Jori, C. Fabris, M. Soncin, S. Ferro, O. Coppellotti, D. Dei, L. Fantetti, G. Chiti and G. Roncucci, *Lasers Surg. Med.*, 2006, **38**, 468–481.
6 A. Anas, J. Sobhanan, K. M. Sulfiya, C. Jasmin, P. K. Sreelakshmi and V. Biju, *J. Photochem. Photobiol., C*, 2021, **49**, 100452.
7 B. Babu, J. Mack and T. Nyokong, *Dalton Trans.*, 2023, **52**, 5000–5018.
8 M. Ravikumar, D. Raghav, K. Rathinasamy, A. Kathiravan and E. M. Mothi, *ACS Appl. Bio Mater.*, 2018, **1**, 1705–1716.
9 I. O. Savelyeva, K. A. Zhdanova, M. A. Gradova, O. V. Gradov and N. A. Bragina, *Curr. Issues Mol. Biol.*, 2023, **45**, 9793–9822.
10 R. Bresolí-Obach, I. Gispert, D. G. Peña, S. Boga, Ó. Gulias, M. Agut, M. E. Vázquez and S. Nonell, *J. Biophotonics*, 2018, **11**, e201800054.
11 B. Babu, J. Mack and T. Nyokong, *New J. Chem.*, 2022, **46**, 5288–5295.

12 N. K. Shee and H. J. Kim, *Molbank*, 2023, **2023**, M1669.
13 J. Aaviksoo, A. Freiberg, S. Savikhin, G. F. Stelmakh and M. P. Tsvirko, *Chem. Phys. Lett.*, 1984, **111**, 275–278.
14 R. Bresolí-Obach, J. Torra, R. P. Zanocco, A. L. Zanocco and S. Nonell, *Methods Mol. Biol.*, 2021, **2202**, 165–188.
15 S. M. Safar Sajadi and S. Khoee, *Sci. Rep.*, 2021, **11**, 2832.
16 M. Taniguchi, J. S. Lindsey, D. F. Bocian and D. Holten, *J. Photochem. Photobiol., C*, 2021, **46**, 100401.
17 K. Procházková, Z. Zelinger, K. Lang and R. Kubát, *J. Phys. Org. Chem.*, 2004, **17**, 890–897.
18 G. G. Parra, D. S. Correa, E. Silveira-Alves, L. M. Almeida, M. A. R. Souza, L. De Boni, L. Misoguti, C. R. Mendonça, S. C. Zílio, N. M. Barbosa Neto, I. E. Borissevitch and P. J. Gonçalves, *Spectrochim. Acta, Part A*, 2021, **261**, 120063.
19 R. Koynova, B. Tenchov, L. Wang and R. C. MacDonald, *Mol. Pharmaceutics*, 2009, **6**, 951.
20 A. Sułek, B. Pucelik, M. Kobielusz, A. Barzowska and J. M. Dąbrowski, *Int. J. Mol. Sci.*, 2020, **21**, 8716.
21 B. Babu, R. C. Soy, J. Mack and T. Nyokong, *New J. Chem.*, 2020, **44**, 11006–11012.
22 T. Dai, A. Gupta, C. K. Murray, M. S. Vrahas, G. P. Tegos and M. R. Hamblin, *Drug Resistance Updates*, 2012, **15**, 223.
23 C. Maher and K. A. Hassan, *MBio*, 2023, **14**, e01205-23.
24 T. Goslinski and J. Piskorz, *J. Photochem. Photobiol., C*, 2011, **12**, 304–321.
25 E. Eruslanov and S. Kusmartsev, *Methods Mol. Biol.*, 2010, **594**, 57–72.
26 D. Figueroa, M. Asaduzzaman and F. Young, *J. Pharmacol. Toxicol. Methods*, 2018, **94**, 26–33.
27 N. S. Lebedeva, Y. A. Gubarev, E. S. Yurina, E. N. Smirnova and S. A. Syrbu, *Colloid Polym. Sci.*, 2017, **295**, 2173–2182.
28 H. Koga, T. Hamada and S. Sakaki, *Dalton Trans.*, 2003, 1153–1160.
29 J. X. Soares, Á. Santos, C. Fernandes and M. M. M. Pinto, *Chemosensors*, 2022, **10**(8), 340.
30 R. Bresolí-Obach, J. Torra, R. P. Zanocco, A. L. Zanocco and S. Nonell, *Methods Mol. Biol.*, 2021, **2202**, 165–188.
31 E. Alves, M. A. F. Faustino, M. G. Neves, A. Cunha, J. Tome and A. Almeida, *Future Med. Chem.*, 2014, **6**, 141–164.
32 W. Li, L. Li, H. Xiao, R. Qi, Y. Huang, Z. Xie, X. Jing and H. Zhang, *RSC Adv.*, 2013, **3**, 13417–13421.